

Accepted, December 1, 2005

## Axisymmetric and triaxial MOND density-potential pairs

L. Ciotti

*Dept. of Astronomy, University of Bologna, I-40127 Bologna, Italy*

P. Londrillo

*INAF-Bologna Astronomical Observatory, I-40127 Bologna, Italy*

C. Nipoti

*Dept. of Astronomy, University of Bologna, I-40127 Bologna, Italy*

### ABSTRACT

We present a simple method, based on the deformation of spherically symmetric potentials, to construct explicit axisymmetric and triaxial MOND density-potential pairs. General guidelines to the choice of suitable deformations, so that the resulting density distribution is nowhere negative, are presented. This flexible method offers for the first time the possibility to study the MOND gravitational field for sufficiently general and realistic density distributions without resorting to sophisticated numerical codes. The technique is illustrated by constructing the MOND density-potential pair for a triaxial galaxy model that, in the absence of deformation, reduces to the Hernquist sphere. Such analytical solutions are also relevant to test and validate numerical codes. Here we present a new numerical potential solver designed to solve the MOND field equation for arbitrary density distributions: the code is tested with excellent results against the analytic MOND triaxial Hernquist model and the MOND razor-thin Kuzmin disk, and a simple application is finally presented.

*Subject headings:* gravitation — stellar dynamics — galaxies: structure — methods: analytical — methods: numerical

## 1. Introduction

Milgrom (1983) proposed that the failure of galactic rotation curves to decline in Keplerian fashion outside the galaxies’ luminous body arises not because galaxies are embedded in massive dark halos, but because Newton’s law of gravity has to be modified for fields that generate accelerations smaller than some characteristic value  $a_0$ . Subsequently, in order to solve basic problems presented by this phenomenological formulation of the theory (now known as Modified Newtonian Dynamics or MOND), such as conservation of linear momentum (Felten 1984), Bekenstein & Milgrom (1984) substituted the heuristic 1983 model with the MOND non-relativistic field equation

$$\nabla \cdot \left[ \mu \left( \frac{\|\nabla\phi\|}{a_0} \right) \nabla\phi \right] = 4\pi G\rho, \quad (1)$$

where  $\|\dots\|$  is the standard Euclidean norm,  $\phi$  is the gravitational potential produced by the density distribution  $\rho$ , and  $\nabla\phi \rightarrow 0$  for  $\|\mathbf{x}\| \rightarrow \infty$ . As stressed by Bekenstein & Milgrom (1984), the equation above is obtained from a variational principle applied to a Lagrangian with all the required symmetries, so the standard conservation laws are obeyed. Thus, equation (1) plays in MOND the same role as the Poisson equation

$$\nabla^2\phi_N = 4\pi G\rho \quad (2)$$

in Newtonian gravity, and the MOND gravitational field  $\mathbf{g}$  experienced by a *test* particle is

$$\mathbf{g} = -\nabla\phi. \quad (3)$$

As well known, in the regime of intermediate accelerations the function  $\mu$  is not fully constrained by theory or observations, while in the asymptotic regimes

$$\mu(t) \sim \begin{cases} t & \text{for } t \ll 1, \\ 1 & \text{for } t \gg 1. \end{cases} \quad (4)$$

Throughout the paper we conform to the standard assumption

$$\mu(t) = \frac{t}{\sqrt{1+t^2}} \quad (5)$$

(see however Famaey & Binney 2005).

From equation (4) it follows that equation (1) reduces to the Poisson equation when  $\|\nabla\phi\| \gg a_0$ , while the limit equation

$$\nabla \cdot (\|\nabla\phi\| \nabla\phi) = 4\pi G a_0 \rho, \quad (6)$$

obtained by assuming  $\mu(t) = t$  in equation (1), describes systems for which (or regions of space where)  $\|\nabla\phi\| \ll a_0$ , i.e. systems for which the MOND predictions differ most from the Newtonian ones. As a consequence equation (6), characterizing the so-called ‘deep MOND regime’ (hereafter dMOND), is of particular relevance in MOND investigations.

Nowadays a considerable body of observational data seems to support MOND well beyond its originally intended field of application (see, e.g., Milgrom 2002; Sanders & McGaugh 2002), making this theory an interesting alternative to the Cold Dark Matter paradigm. It is thus natural to study in detail MOND predictions, in particular focusing on dMOND systems, i.e. systems that should be dark matter dominated if Newtonian gravity holds. Potential problems of the theory have already been pointed out by various authors (see, e.g. The & White 1988; Buote et al. 2002; Sanders 2003; Ciotti & Binney 2004; Knebe & Gibson 2004; Zhao et al. 2005), but further analyses are needed to reach firmer conclusions. Unfortunately, MOND investigations have been considerably slowed down by the lack of aspherical density-potential pairs to test theory predictions in cases more realistic than those described by spherical symmetry: the search for a sufficiently general method to construct aspherical MOND solutions is the subject of this paper.

In MOND, the main difficulty to obtain exact aspherical density-potential pairs (or to build robust numerical solvers) originates from the non-linear nature of the theory, which makes impossible a straightforward use of the analytical and numerical techniques available for the Poisson equation (such as integral transforms or expansion in orthogonal functions). In addition, a simple relation between the Newtonian and the MOND gravity fields in general does not exist. Although equation (2) can be used to lower the order of equation (1) by eliminating the source density, it follows that  $\mu(\|\nabla\phi\|/a_0)\nabla\phi$  and  $\nabla\phi_N$  differ by some unknown solenoidal field<sup>1</sup>  $\mathbf{S} = \text{curl } \mathbf{h}$ . Remarkably, Brada & Milgrom (1995; hereafter BM95) showed that when the modulus  $g_N$  of the Newtonian gravitational field produced by  $\rho$  is a function of  $\phi_N$  only,  $\mathbf{S}$  vanishes, and so the MOND acceleration  $\mathbf{g}$  is related to  $\mathbf{g}_N \equiv -\nabla\phi_N$  by

$$\mu\left(\frac{g}{a_0}\right)\mathbf{g} = \mathbf{g}_N, \quad (7)$$

where  $g = \|\mathbf{g}\|$ . Equation (7) coincides with the original MOND formulation of Milgrom

---

<sup>1</sup>That the solenoidal field  $\mathbf{S}$  in general cannot be arbitrarily set to zero is due to the fact that the MOND acceleration field must be derived from a potential, while equation (7), if correct in general, would imply that  $\nabla\|\mathbf{g}\| \wedge \mathbf{g} = 0$ , an identity which is not necessarily true when  $\mathbf{g}$  is derived from a potential.

(1983) and can be solved algebraically: particularly simple cases described by this equations are those in which the density distribution is spherically or cylindrically symmetric, or stratified on homogeneous planes. In such cases the MOND potential is not more difficult to construct than the corresponding Newtonian potential. This is the reason why *all* the (astrophysically relevant) analytical MOND density-potential pairs known are spherically symmetric: in fact, the only exact, aspherical MOND density-potential pair available is the axisymmetric razor-thin Kuzmin disk (and the derived family; BM95), for which  $g_N = g_N(\phi_N)$ . In all the other cases one is forced to solve numerically equation (1).

The importance of a general method to obtain the explicit MOND potential of density distributions with prescribed shape and stratification is then obvious, because it would allow for orbit integration, without resorting to numerical integration of equation (1); in addition, analytical solutions could be used to test numerical MOND solvers in more realistic cases than spherical symmetry. In this paper we show that such an approach can be devised. In particular, we show how a “seed” spherical density distribution can be deformed in an axisymmetric or triaxial density distribution with analytical potential satisfying the MOND equation, by means of a pair of very simple existence theorems and (for example) by using building blocks obtained from the Ciotti & Bertin (2005; hereafter CB05) method. In addition, as a complement to the analytical method, we also illustrate a new numerical MOND solver based on spectral methods, which adds to the short list of the others available (Milgrom 1986; BM95; see also Brada & Milgrom 1999).

The paper is organized as follows. In Section 2 we present the general method (postponing to the Appendix the proof of three technical results on which the method is based), and in Section 3 we construct families of triaxial profiles obtained by deformation of the Hernquist (1990) sphere. The original numerical code developed to compute the MOND potential of generic density distributions is then described in Section 4, where we also show how well it recovers the analytical triaxial potentials of Section 3 and the MOND Kuzmin density-potential pair. The code is finally used to investigate the field  $\mathbf{S}$  of highly flattened triaxial density distributions. The main results of the paper and possible future applications are finally summarized in Section 5.

## 2. The general method

Two different approaches are possible to construct explicit solutions of equation (1): in the most obvious one attempts to recover the potential of a given density  $\rho$ . Unfortunately, no explicit aspherical density-potential pairs (with the exception of the Kuzmin disk) have been obtained so far following this approach. In addition, we note that even “innocent” density distributions can produce puzzling behaviors of the MOND acceleration field at special places, as illustrated by the perturbative case analyzed by Ciotti & Binney (2004).

In the alternative “ $\phi$ -to- $\rho$ ” approach – studied in this paper – one determines the density field by application of the MOND operator to a prescribed potential<sup>2</sup>. This approach is straightforward because only differentiation is involved, but negative densities can be produced if the potential is chosen without the necessary care, as well known also in the Newtonian case. Thus, a first problem posed by this approach is to find a criterion to choose  $\phi$  such that  $\rho$  is positive. In addition to the positivity condition, one would like to be able to control the *shape* and the *radial trend* of the resulting density distribution: for example, in Newtonian gravity homeoidally stratified potentials lead to curious toroidal density distributions (e.g. Binney 1981, Evans 1994). As we will see, it is possible – to some degree – to answer positively to these issues.

The idea behind our method is to compute the MOND potential of a spherical density distribution. The obtained potential is then mapped on a new spherical density by means of the Laplace operator. This new density is then suitably deformed and the associated (Newtonian) potential is determined by standard methods. Finally, the MOND differential operator is applied to the deformed potential, and the final density distribution is obtained. In practice, the method consists of the following steps.

1) We start by selecting a spherical density distribution  $\rho_0(r)$  with the desired radial behavior: for example, it could be a  $\gamma$ -model (Dehnen 1993; Tremaine et al. 1994), a King (1972) density distribution, or a classical polytrope such as the Plummer (1911) sphere. We then calculate its dMOND potential  $\phi_0(r)$  by using equation (7) in spherical symmetry:

$$\frac{d\phi_0}{dr} = g_0 = \frac{\sqrt{GM_0(r)a_0}}{r}, \quad (8)$$

where  $M_0(r) = 4\pi \int_0^r \rho_0(r)r^2 dr$ . As is well known,  $\phi_0(r \rightarrow \infty) \sim \sqrt{GM_0 a_0} \ln r$  for any mass

---

<sup>2</sup>A first attempt to construct the MOND potential of an oblate galaxy along this line was carried out by Hongsheng Zhao (private communication).

distribution of finite total mass  $M_0$ . We stress that we are calculating the dMOND potential of  $\rho_0$  irrespective of whether the density distribution is actually dMOND everywhere: for example, the Jaffe (1983) model near the center is not dMOND because its acceleration field diverges there, yet we can integrate equation (8) to obtain  $\phi_0$ . The reasons for doing so are that equation (8) is much easier to integrate than the corresponding MOND (spherically symmetric) equation, and that Theorem 2 assures that both the Laplacian and the MOND operator applied to  $\phi_0$  will produce positive densities. In particular, the Laplace operator applied to  $\phi_0$  leads to the density distribution

$$\rho_{N0} = \sqrt{\frac{a_0}{G}} \left[ \frac{\rho_0(r)r}{2\sqrt{M_0(r)}} + \frac{\sqrt{M_0(r)}}{4\pi r^2} \right], \quad (9)$$

while the MOND operator in equation (1) produces

$$\rho_{M0} = \mu \left( \frac{g_0}{a_0} \right) \left[ \rho_{N0} + \frac{g'_0}{4\pi G (1 + g_0^2/a_0^2)} \right]. \quad (10)$$

By construction  $\phi_0$  is the dMOND potential of  $\rho_0$ , the Newtonian potential of  $\rho_{N0}$ , and the MOND potential of  $\rho_{M0}$ . Obviously,  $\rho_{M0}$  coincides with  $\rho_0$  where the model is in dMOND regime, and with  $\rho_{N0}$  where the gravity field  $g_0$  is strong enough. From a more quantitative point of view,  $\rho_{N0}(r \rightarrow \infty) \propto r^{-2}$  when the total mass of  $\rho_0$  is finite, and  $\rho_{N0}(r \rightarrow 0) \propto r^{-(1+a)/2}$  if  $\rho_0 \propto r^{-a}$  ( $a < 3$ ) in the central regions. This is apparent from Fig. 1, where we plot  $\rho_0$  (solid lines),  $\rho_{N0}$  (dashed lines) and  $\rho_{M0}$  (empty symbols) for  $\gamma$ -models with  $\gamma = 0, 1$ , and  $2$ .

2) In the second step of the procedure we look for an aspherical density  $\rho_{N1}$  to be added to  $\rho_{N0}$  so that  $\rho_{N0} + \lambda\rho_{N1}$  is positive for some  $\lambda > 0$ , and  $\phi_1$  (defined by  $\nabla^2\phi_1 = 4\pi G\rho_{N1}$ ) is explicitly known. The associated total (Newtonian) potential is thus  $\phi = \phi_0 + \lambda\phi_1$ . The main reason for working with Newtonian potential at this stage is that the properties of density-potential pairs obeying the Poisson equation are well known, and so we can work with confidence and control the deformations of the total  $\rho_{N0} + \lambda\rho_{N1}$ .

3) The final step is the explicit evaluation of the dMOND operator in equation (6) for the potential  $\phi = \phi_0 + \lambda\phi_1$ , and this can be done with computer algebra packages such as Maple or Mathematica. For  $\lambda = 0$  one recovers  $\phi_0$  (which produces the positive  $\rho_0$ ), and for continuity one could expect that a positive  $\rho$  (with a radial trend similar to that of  $\rho_0$ ) is also obtained for sufficiently small  $\lambda$ , though we will show that this is not always the case<sup>3</sup>.

---

<sup>3</sup>See the discussion below equation (15).

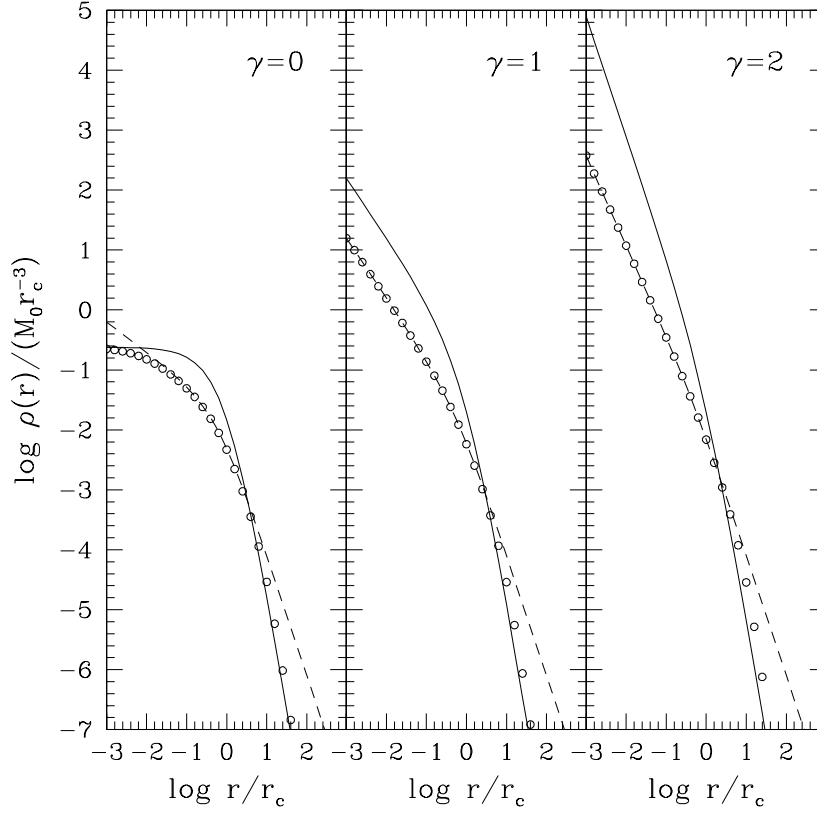


Fig. 1.— The Newtonian (dashed lines) density profile  $\rho_{N0}$  [equation (9)] and the full MOND (empty symbols) density profile  $\rho_{M0}$  [equation (10)] derived from the dMOND potential of the spherical  $\gamma$ -model  $\rho_0 = (3 - \gamma)M_0 r_c / [4\pi r^\gamma (r + r_c)^{4-\gamma}]$  for  $\gamma = 0, 1, 2$  (solid lines). In all cases we adopted  $GM_0 = 100a_0 r_c^2$ .

In general, for given  $\rho$  and  $\rho_{\text{N1}}$  a critical value of  $\lambda$  exists such that only smaller values  $\lambda$  correspond to physically acceptable (i.e. nowhere negative)  $\rho$ . If the resulting density is positive, then Theorem 1 assures us that also the full MOND operator applied to  $\phi$  will produce a positive density distribution (such that its limit for  $\lambda \rightarrow 0$  is  $\rho_{\text{M0}}$ ), provided that  $\rho_{\text{N0}} + \lambda\rho_{\text{N1}} \geq 0$ . Note that the last requirement is just a *sufficient* condition for the positivity of  $\rho$ .

A first hint about the positivity and the shape of the resulting density can be obtained by studying the linearization of the dMOND operator. In fact, it is easy to prove that the  $\lambda$ -linearized density associated with  $\phi = \phi_0 + \lambda\phi_1$  is

$$\rho = \rho_0 + \frac{\lambda}{4\pi G a_0} \left[ \left( 4\pi G \rho_{\text{N1}} + \frac{\partial^2 \phi_1}{\partial r^2} \right) g_0 + \left( 4\pi G \rho_{\text{N0}} + \frac{d^2 \phi_0}{dr^2} \right) \frac{\partial \phi_1}{\partial r} \right] + O(\lambda^2), \quad (11)$$

where the spherical symmetry of  $\phi_0$  has been exploited by using the standard spherical coordinates  $(r, \vartheta, \varphi)$ , and it is intended that  $\phi_1 = \phi_1(r, \vartheta, \varphi)$  and  $g_0 \neq 0$ .

From the discussion above it should be obvious that the delicate step in the procedure is the choice of  $\rho_{\text{N1}}$  such that  $\rho_{\text{N0}} + \lambda\rho_{\text{N1}}$  is nowhere negative,  $\phi_1$  is analytical, and the dMOND operator produces the sought deformation on  $\rho$ . Simple choices satisfying the first two requests could be the addition of Miyamoto & Nagai (1975) or Satho (1980) disks: however, an even more general approach can be devised. In fact, families of explicit and easy-to-calculate Newtonian  $(\rho_{\text{N1}}, \phi_1)$  pairs can be obtained from the homeoidal expansion technique (e.g., see CB05). In practice, for the present problem one can adopt as  $\rho_{\text{N1}}$  the linear term in the homeoidal expansion of a *seed density*  $\varrho$ , i.e.

$$\rho_{\text{N1}} = (\epsilon y^2 + \eta z^2) \frac{\varrho'(r)}{r}, \quad (12)$$

where the dimensionless parameters  $\epsilon$  and  $\eta$  are the flattenings of the expanded homeoidal density distribution. The potential  $\phi_1$  generated by the distribution  $\rho_{\text{N1}}$  is written in terms of one-dimensional radial integrals that usually can be evaluated explicitly (see equations [5] and [6] in CB05):

$$\frac{\phi_1}{4\pi G} = (\epsilon + \eta)\psi_1(r) + (\epsilon y^2 + \eta z^2)\psi_2(r), \quad (13)$$

where

$$\psi_1(r) = \int_0^r \frac{\varrho(m)m^2}{r} \left( 1 - \frac{m^2}{3r^2} \right) dm + \frac{2}{3} \int_r^\infty \varrho(m)m dm, \quad (14)$$

and

$$\psi_2(r) = \frac{1}{r^5} \int_0^r \varrho(m)m^4 dm. \quad (15)$$



We stress that in the present application  $\epsilon$  and  $\eta$  are just linear parameters, so without loss of generality the multiplicative coefficient  $\lambda$  can be considered to be contained in them, and their value is not restricted by the limitations described in appendix A of CB05. Note also that  $\rho_{N1}$  in equation (12) is *negative* when it is derived from an *oblate* axisymmetric (the  $\epsilon = 0$  case) or triaxial  $\varrho$ , and so particular care is needed in the choice of  $\varrho$ , in order to have  $\rho_{N0} + \rho_{N1} \geq 0$ . However, for a  $\varrho$  that can be approximated by a power-law in its external regions,  $\rho_{N1}(r \rightarrow \infty) \sim -\varrho$ , and so any finite-mass  $\varrho$  produces through equation (12) a positive total density at large radii, where  $\rho_{N0} \sim r^{-2}$ . Finally we remark that, for  $\rho_{N1}$  as in equation (12), the quantities  $\partial\phi_1/\partial r$  and  $\partial^2\phi_1/\partial r^2$  in equation (11) are particularly simple because, according to equation (13), the angular part of  $\phi_1$  is just a multiplicative factor of the radial function  $r^2\psi_2$ .

We note that the seemingly obvious choice of taking  $\rho_{N1}$  to be the homeoidal expansion term derived from  $\rho_{N0}$ , does not work. This is because  $\rho_{N0} \sim r^{-2}$  at large radii, so  $\rho_{N1} \propto -(\epsilon \sin^2 \vartheta \sin^2 \varphi + \eta \cos^2 \vartheta)/r^2$  and  $\phi_1 \propto -2(\epsilon + \eta) \ln r/3 + (\epsilon \sin^2 \vartheta \sin^2 \varphi + \eta \cos^2 \vartheta)/3$  for  $r \rightarrow \infty$ : equation (11) then reveals that the density is negative for sufficiently large  $r$  in the conical region  $\cos \vartheta < 1/\sqrt{3}$ . As we will see, the regions near the  $z$  axis are in fact the most delicate when applying the analytical technique presented in this paper: unphysical models usually develop negative densities near the  $z$ -axis.

We conclude this Section by noting that, when truncated at the first order in  $\lambda$ ,  $\phi_0 + \lambda\phi_1$  and the  $\lambda$ -linearized  $\rho$  in equation (11) allow for the explicit evaluation of the  $\lambda$ -linearized solenoidal field  $\mathbf{S} = \|\nabla\phi\|\nabla\phi/a_0 - \nabla\phi_N = \lambda\mathbf{S}_1 + O(\lambda^2)$  (the zeroth-order term in  $\lambda$  is obviously missing because it refers to the spherical density component). If  $\phi_1$  is given by equation (13) then  $\rho$  in equation (11) belongs to the family considered in CB05 and its Newtonian potential can be derived in closed form (while in general this is not possible when considering the density obtained by the application of the dMOND operator without  $\lambda$ -linearization).

### 3. A simple application: triaxial Hernquist galaxy

In order to illustrate the method described in Section 2 we now construct a triaxial galaxy model with a realistic density distribution and analytical MOND potential.

Following Step 1, we start with the spherically symmetric Hernquist (1990) density

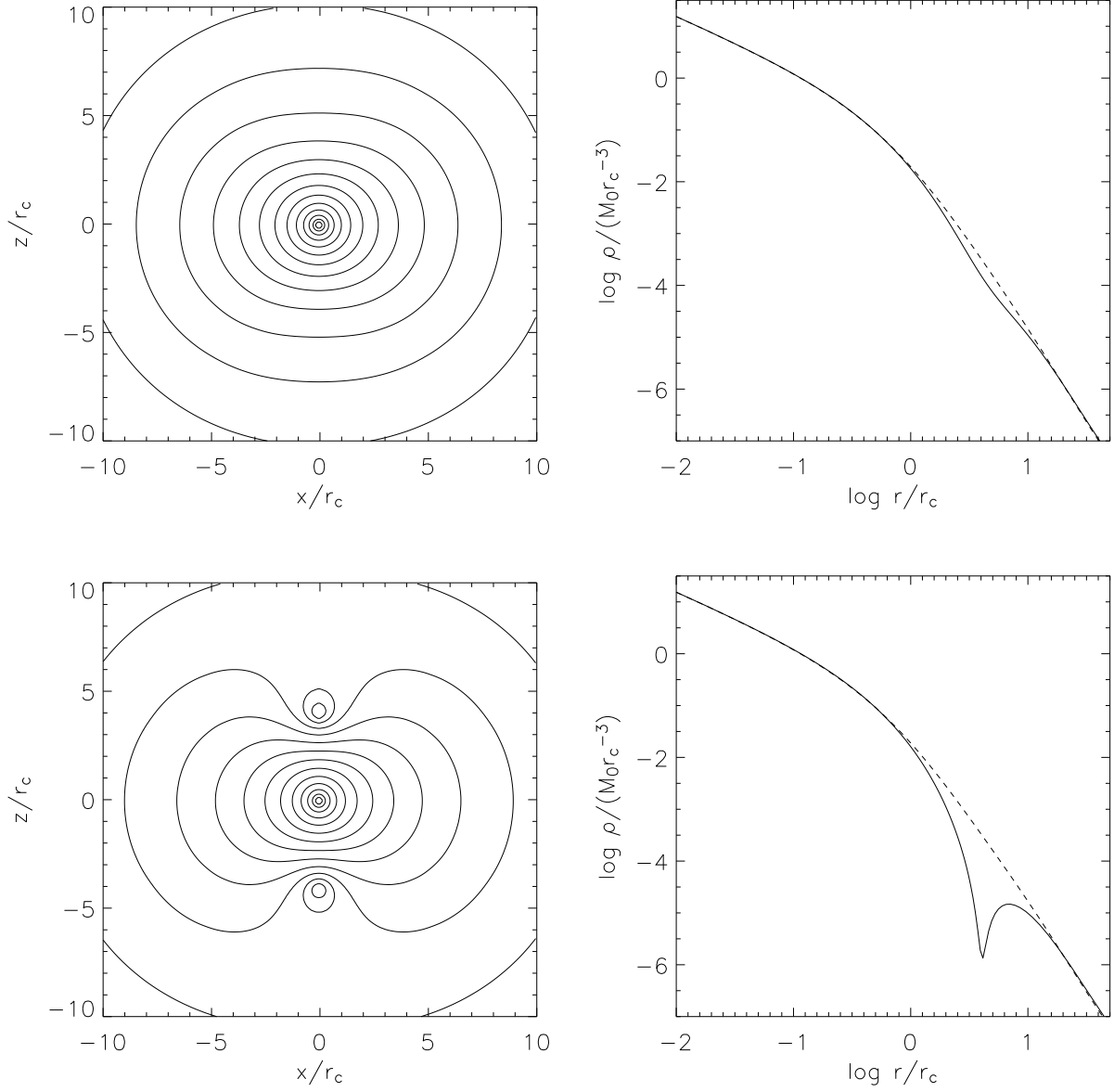


Fig. 2.— Isodensity contours (left panels) and density profiles (right panels) for two analytical dMOND axisymmetric ( $\epsilon = 0$ ) Hernquist models with  $\phi_1$  as in equation (21). The density profiles are taken along a radius in the equatorial plane (dashed lines) and along the symmetry axis  $z$  (solid lines). The model in the top panels has  $\beta = 5$  and  $\tilde{\eta} = 0.01$ , while the model in the bottom panels has  $\beta = 5$  and  $\tilde{\eta} = 0.02$ .

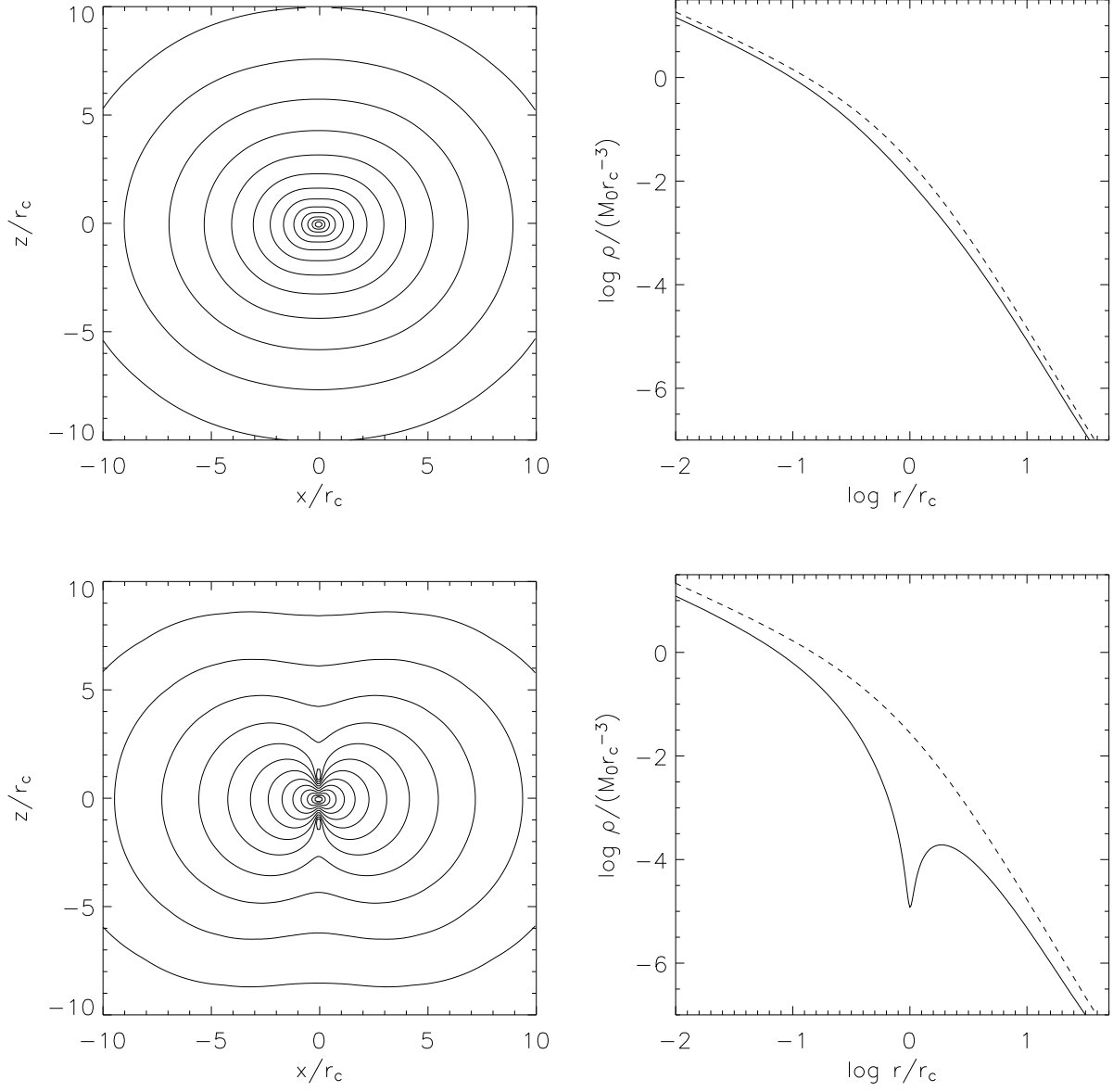


Fig. 3.— The same quantities as in Fig. 2 for two analytical dMOND axisymmetric ( $\epsilon = 0$ ) Hernquist models with  $\phi_1$  as in equation (24), with  $\eta = 0.2$  (top) and  $\eta = 0.4$  (bottom).

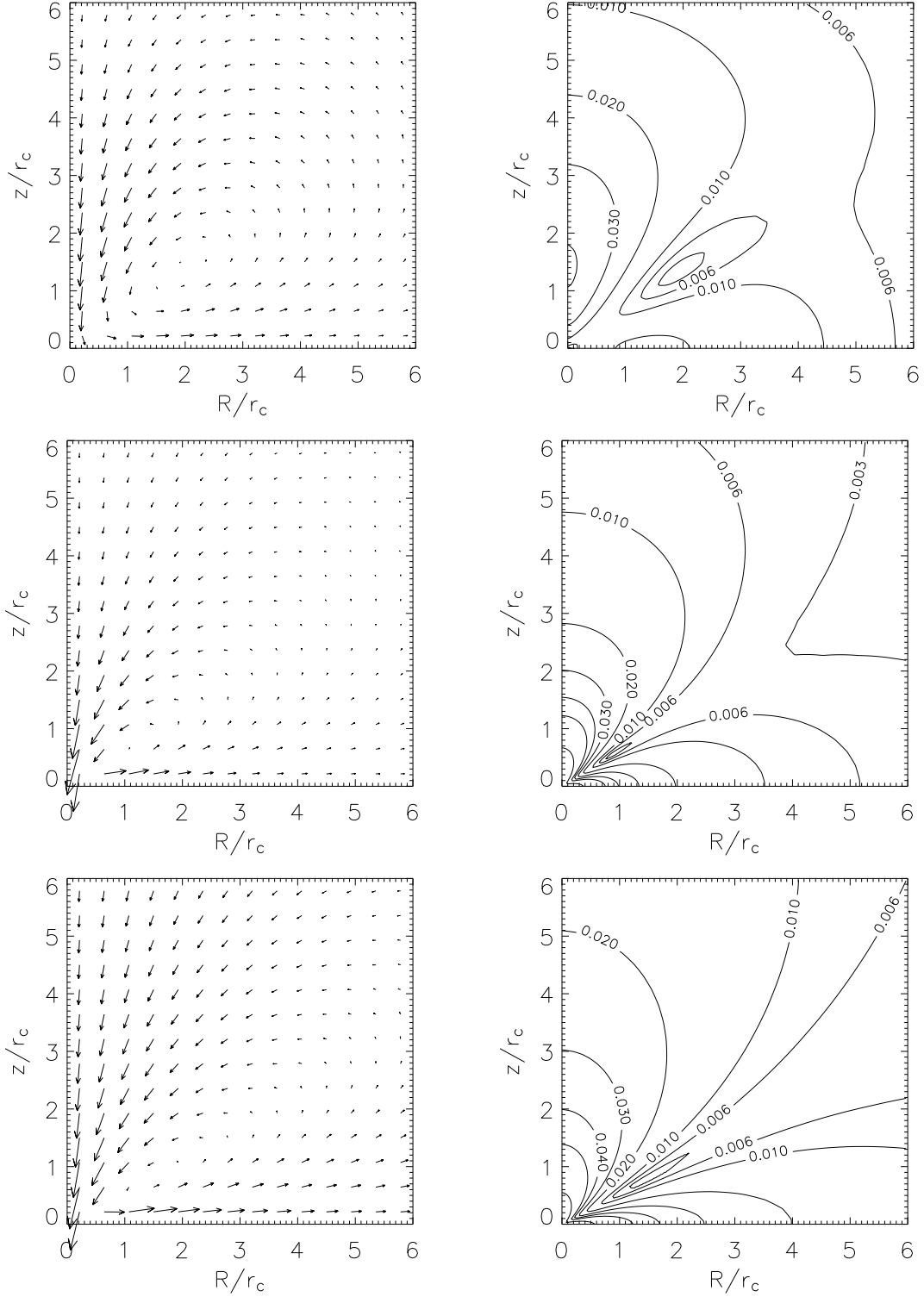


Fig. 4.— The dMOND solenoidal field  $\mathbf{S} \equiv g\mathbf{g}/a_0 - \mathbf{g}_N$  (normalized to  $g_N$ ) in the meridional plane for three different axisymmetric Hernquist models (left panels). In the right panels lines of constant  $\|\mathbf{S}\|/g_N$  are shown. From top to bottom: the model of Fig. 2 with  $\tilde{\eta} = 0.02$ , the model of Fig. 3 with  $\eta = 0.4$ , and the homeoidally stratified axisymmetric Hernquist model [equation (37)] with  $\epsilon = 0$  and  $\eta = 0.5$ .

distribution

$$\rho_0(r) = \frac{M_0}{2\pi r_c^3} \frac{1}{s(1+s)^3}, \quad (16)$$

where  $s \equiv r/r_c$ ; we recall that this density distribution, when projected, is a good approximation of the  $R^{1/4}$  law (de Vaucouleurs 1948) over a large radial interval, thus providing a realistic description of the luminous density distribution of elliptical galaxies. From equation (8)  $g_0 = \sqrt{GM_0 a_0}/r_c(1+s)$ , and so the dMOND potential is

$$\phi_0 = \sqrt{GM_0 a_0} \ln(1+s), \quad (17)$$

while from equation (9)

$$\rho_{N0} = \frac{\sqrt{GM_0 a_0}}{4\pi G r_c^2} \frac{s+2}{s(s+1)^2}. \quad (18)$$

In agreement with the discussion in Section 2,  $\rho_{N0} \sim \rho_0 \sim r^{-1}$  in the central regions and  $\rho_{N0} \propto r^{-2}$  in the outer parts of the dMOND Hernquist model.

According to Step 2, we look for a density distribution  $\rho_{N1}$  to be added to  $\rho_{N0}$  such that the total density is positive and the potential  $\phi_1$  is explicitly known. A family of densities that can be easily expanded with the CB05 technique and admit a simple analytical potential  $\phi_1$  is

$$\varrho(r) = \frac{\varrho_0 \beta^a}{(s+\beta)^a}, \quad (a > 3), \quad (19)$$

where  $\varrho_0$  is a density scale, and  $\beta$  is the scale-length in units of  $r_c$ . There is nothing special about the distribution (19), which has been chosen only by simplicity arguments: note however that at both small and large radii the total density is dominated by  $\rho_{N0}$ , so its positivity has to be checked only for the intermediate regions. Here we restrict to the case  $a = 6$  (see also Muccione & Ciotti 2004), and from equation (12)

$$\rho_{N1} = -6\varrho_0 \beta^6 \frac{(\epsilon \sin^2 \vartheta \sin^2 \varphi + \eta \cos^2 \vartheta)s}{(s+\beta)^7}, \quad (20)$$

so that

$$\phi_1 = 4\pi G \varrho_0 \beta^5 r_c^2 \left[ \frac{(\epsilon + \eta)(s^2 + 3\beta s + \beta^2)}{30\beta^2(s+\beta)^3} + \frac{(\epsilon \sin^2 \vartheta \sin^2 \varphi + \eta \cos^2 \vartheta)s^2}{5(s+\beta)^5} \right]. \quad (21)$$

Before computing the dMOND operator for  $\phi_0 + \phi_1$  it is worth studying its linearization for  $\epsilon \rightarrow 0$  and  $\eta \rightarrow 0$ , and from equation (11) we obtain

$$\begin{aligned} \frac{\rho_c^3}{M_0} \simeq & \frac{1}{2\pi s(s+1)^3} + \beta^3(\tilde{\epsilon} + \tilde{\eta}) \frac{s^5 + 7\beta s^4 + 9\beta^2 s^3 + \beta^2(\beta-6)s^2 - 2\beta^3(\beta+6)s - 6\beta^4}{15(s+1)^2(s+\beta)^7} + \\ & 6\beta^5(\tilde{\epsilon} \sin^2 \vartheta \sin^2 \varphi + \tilde{\eta} \cos^2 \vartheta) \frac{6s^3 - (23\beta - 3)s^2 + \beta(\beta - 24)s + 3\beta^2}{15(s+1)^2(s+\beta)^7}, \end{aligned} \quad (22)$$

where the new dimensionless parameters  $\tilde{\epsilon}$  and  $\tilde{\eta}$  are defined as  $\tilde{\epsilon}/\epsilon = \tilde{\eta}/\eta = \varrho_0 r_c^2 \sqrt{G/M_0 a_0}$ . Thus,  $\rho \sim \rho_0 \sim r^{-1}$  for  $r \rightarrow 0$ , while for  $r \rightarrow \infty$

$$\frac{\rho r_c^3}{M_0} \simeq \left( \frac{1}{2\pi} + \beta^3 \frac{\tilde{\epsilon} + \tilde{\eta}}{15} \right) \frac{1}{s^4} + 12\beta^5 \frac{\tilde{\epsilon} \sin^2 \vartheta \sin^2 \varphi + \tilde{\eta} \cos^2 \vartheta}{5s^6}, \quad (23)$$

i.e., the linearized density retains the spherical symmetry and radial trend of  $\rho_0$  for  $r \rightarrow 0$  and  $r \rightarrow \infty$ , so negative values of  $\rho$  can be present at intermediate distances only from the center. For instance, restricting to the axisymmetric case ( $\epsilon = 0$ ) with  $\beta = 5$ , according to equation (22) negative values of  $\rho$  first appear for  $\tilde{\eta} \gtrsim 0.018$  along the  $z$ -axis near  $z \sim 4r_c$ , and smaller values of  $\tilde{\eta}$  correspond to an everywhere positive  $\rho$ .

The formula resulting from the evaluation of the dMOND operator is not reported here, and we limit ourselves to show the isodensity contours in a pair of representative axisymmetric ( $\epsilon = 0$ ) cases, fixing  $\beta = 5$ . In Fig. 2 (top left panel) we show the isodensity contours in the meridional plane for the model with  $\tilde{\eta} = 0.01$ . Note how the density is spherically symmetric both in the central regions and at large distances, in accordance with equation (22). It is particularly important to stress that the maximum flattening of the density corresponds to an axis ratio  $\sim 0.8$ , even though  $\tilde{\eta}$  is much smaller than 0.2. This is at variance with the Newtonian case (in which the flattening of the expanded density is the same as that of the seed density for small deformations), and this is a result of the non-linear nature of MOND. In the top right panel of Fig. 2 we show the density profiles along the symmetry axis (solid line) and along a radius in the equatorial plane (dashed line) for the same model. It is apparent how the radial trend of the spherical Hernquist model has been nicely preserved by the imposed deformation, again in accordance with equation (22). Note, however, how the density profile along the  $z$  axis shows a small depression, which becomes more apparent in the model  $\tilde{\eta} = 0.02$  (Fig. 2, lower panels). This last model is near the consistency limit in  $\tilde{\eta}$ , and the axis ratio of the flattest isodensity surface is  $\sim 0.6$ . Larger values of  $\tilde{\eta}$  would produce a negative density along the  $z$  axis at  $z \sim 4r_c$ , in agreement with the results of the linear analysis.

It should be clear that the presented model is just one of the many analytical triaxial Hernquist models one can construct. For example, one could adopt the  $\phi_1$  derived from the homeoidal expansion of a power-law  $\varrho$  (CB05), or just add a quadrupole potential [i.e., assume  $\psi_1 = 0$  in equation (13)]. For instance, in Fig. 3 we show the density obtained by evaluating the dMOND density of the potential  $\phi_0 + \phi_1$ , where  $\phi_0$  is still given by equation (17),

but

$$\phi_1 = \sqrt{GM_0 a_0} \frac{(\epsilon \sin^2 \vartheta \sin^2 \varphi + \eta \cos^2 \vartheta) s}{(s + \beta)^2} \quad (24)$$

The two models shown are characterized by  $\epsilon = 0$ ,  $\beta = 1$ ,  $\eta = 0.2$  (top) and  $\eta = 0.4$  (bottom). Overall, we can note that for these models the isodensity surfaces are flat also in the central regions and in the models outskirts, and that the symmetry axis is again the region where the model becomes unphysical for too large  $\eta$ .

We conclude this Section discussing briefly the global properties of the dMOND field  $\mathbf{S} = g\mathbf{g}/a_0 - \mathbf{g}_N$  for the presented models. In Fig. 4 (left) we show the field  $\mathbf{S}/g_N$  in the meridional plane, while in the right panels we plot lines of constant  $S/g_N$ , where  $S \equiv \|\mathbf{S}\|$  (The Newtonian field  $\mathbf{g}_N$  has been evaluated numerically with a spectral Poisson solver; see Section 4). The quantity  $S/g_N$  gives direct information about the relative importance of the solenoidal field with respect to the Newtonian gravitational field. Remarkably, as already pointed out by BM95, also in our case the solenoidal field is typically almost everywhere much smaller than  $g_N$ : we find  $S/g_N \lesssim 0.05$  for the family of axisymmetric and triaxial models obtained from equation (21). However, we also find that this is not necessarily the rule: for example,  $S/g_N \sim 0.25$  in the central regions of the models obtained from equation (24), and other cases of non-negligible solenoidal field will be discussed in the next Section.

#### 4. The numerical MOND potential solver

The results presented in the previous Sections, albeit encouraging, suggest that in order to have a full control on the density field producing the MOND potential the best tool is still the numerical solution of equation (1). To our knowledge the only MOND numerical solvers presently available are the two-dimensional code developed by Milgrom (1986), and the BM95 three-dimensional, multi-grid solver [used by Brada & Milgrom (1999) in their N-body code]. Here, as a complement to the analytical method, we present a new numerical three-dimensional MOND potential solver based on a spherical coordinates grid, which can be easily implemented in a standard particle-mesh N-body code.

The goal is to solve numerically equation (1) for  $\phi(\mathbf{x})$ , i.e. the non-linear elliptic boundary value problem defined by

$$\hat{M}[\phi(\mathbf{x})] \equiv \nabla \cdot \left[ \mu \left( \frac{g}{a_0} \right) \nabla \phi(\mathbf{x}) \right] - 4\pi G \rho(\mathbf{x}) = 0, \quad g = O(r^{-1}) \text{ for } r \rightarrow \infty, \quad (25)$$

where  $\mathbf{x} = (x, y, z)$ ,  $r \equiv \|\mathbf{x}\|$ ,  $\rho(\mathbf{x})$  is assigned, and  $g = \|\mathbf{g}\|$  with  $\mathbf{g} = -\nabla \phi(\mathbf{x})$ .

The numerical scheme is based on the iterative Newton method, which is robust and relatively simple to implement. At the  $(n + 1) - th$  iteration we indicate with  $\delta\phi^{(n)}$  the increment function to be determined so that  $\phi^{(n+1)} = \phi^{(n)} + \delta\phi^{(n)}$  is a better approximation of the solution, while  $\phi^{(n)}$  and  $g^{(n)} = -\nabla\phi^{(n)}$  are quantities known from the previous iteration. In our case,  $\delta\phi^{(n)}$  is the solution of the linear equation

$$\delta\hat{M}^{(n)} [\delta\phi^{(n)}] = -\hat{M} [\phi^{(n)}], \quad (26)$$

where the linear operator

$$\delta\hat{M}^{(n)} \equiv \nabla \cdot [\mu^{(n)} \nabla + \mu'^{(n)} \mathbf{g}^{(n)} (\mathbf{g}^{(n)} \cdot \nabla)] \quad (27)$$

satisfies the identity

$$\hat{M} [\phi^{(n+1)}] - \hat{M} [\phi^{(n)}] = \delta\hat{M}^{(n)} [\delta\phi^{(n)}] + O [(\delta\phi^{(n)})^2], \quad (28)$$

where  $\mu^{(n)} \equiv \mu(g^{(n)}/a_0)$  and  $\mu'^{(n)} \equiv \mu'(g^{(n)}/a_0)/g^{(n)}a_0$  are known. Equation (26) is solved by inversion of  $\delta\hat{M}^{(n)}$ , and the procedure is repeated until numerical convergence to the solution  $\phi_{\text{num}}$  (defined by  $\max |\hat{M}[\phi_{\text{num}}]| < \varepsilon$ , where  $\varepsilon$  is a prescribed tolerance) is attained.

The solution of equation (26) requires in general a finite difference approximation of the spatial derivatives and the inversion of a three-dimensional matrix. Note that boundedness of the inverse of the operator  $\delta\hat{M}^{(n)}$  assures quadratic convergence of the scheme for  $\phi^{(0)}$  sufficiently close to the sought solution (e.g. Stoer & Bulirsch 1980). In our implementation, designed for finite mass distributions, we represent equation (25) and (26) in spherical coordinates, which allow for a simple assignment of the boundary conditions. Moreover, we approximate the linear operator (27) with

$$\delta\hat{\mathcal{M}}^{(n)} \equiv \frac{1}{r^2} \left[ \frac{\partial}{\partial r} \left( r^2 \bar{\mu}^{(n)}(r) \frac{\partial}{\partial r} \right) + \bar{\mu}^{(n)}(r) (\hat{L}_\vartheta + \hat{L}_\varphi) \right], \quad (29)$$

where

$$\hat{L}_\vartheta \equiv \frac{1}{\sin \vartheta} \frac{\partial}{\partial \vartheta} \left( \sin \vartheta \frac{\partial}{\partial \vartheta} \right), \quad \hat{L}_\varphi \equiv \frac{1}{\sin \vartheta} \frac{\partial^2}{\partial \varphi^2} \quad (30)$$

are the angular components of the Laplace operator,  $\bar{\mu}^{(n)}(r) = (1/4\pi) \int \mu^{(n)}(r, \vartheta, \varphi) \sin \vartheta d\vartheta d\varphi$ , and the variation  $\mu^{(n+1)} - \mu^{(n)} \propto \mu'^{(n)}$  is neglected. It is easy to show that with this new operator quadratic convergence in equation (26) is replaced by linear convergence since

$$\hat{M} [\phi^{(n+1)}] - \hat{M} [\phi^{(n)}] = \delta\hat{\mathcal{M}}^{(n)} [\delta\phi^{(n)}] + O [\delta\phi^{(n)}]. \quad (31)$$



However, the inversion of  $\delta\hat{\mathcal{M}}^{(n)}$  is much simpler because we are now in the position to use the full power of spherical harmonics. In fact, after expanding the source term  $\hat{M}[\phi^{(n)}]$  and the unknown function  $\delta\phi^{(n)}$  in spherical harmonics

$$\delta\phi^{(n)}(r, \vartheta, \varphi) = \sum_{l,m} \delta\phi_{l,m}^{(n)}(r) Y_l^m(\vartheta, \varphi) \quad (32)$$

(e.g. Binney & Tremaine 1987), the modified equation (26) reduces to

$$\frac{1}{r^2} \left[ \frac{\partial}{\partial r} \left( r^2 \bar{\mu}^{(n)} \frac{\partial}{\partial r} \right) - \bar{\mu}^{(n)}(r) l(l+1) \right] \delta\phi_{l,m}^{(n)}(r) = -\hat{M}[\phi^{(n)}]_{l,m}, \quad (33)$$

involving derivatives only in the radial coordinates. The solutions  $\delta\phi_{l,m}^{(n)}(r)$  are back transformed into  $\delta\phi^{(n)}(r, \vartheta, \varphi)$  according to equation (32), and the new components of the acceleration field  $\mathbf{g}^{(n+1)} = \mathbf{g}^{(n)} - \nabla\delta\phi^{(n)}$  are evaluated.

In order to solve equation (33) we introduce the invertible mapping for the radial coordinate

$$r(\xi) = \tan^\alpha \xi, \quad (0 \leq \xi < \pi/2), \quad (34)$$

so that the infinite radial range is mapped onto the finite interval  $[0, \pi/2)$ ,

$$\frac{\partial}{\partial r} = \frac{\cos^2 \xi}{\alpha \tan^{\alpha-1} \xi} \frac{\partial}{\partial \xi}, \quad (35)$$

and the boundary conditions for the radial derivative of the potential at  $\xi = \pi/2$  are automatically satisfied (Londrillo & Messina 1990); in our applications we adopt  $\alpha = 1$  or  $\alpha = 2$ . In practice, the  $(\xi, \vartheta, \varphi)$  coordinates are discretized on a uniform  $(\xi_i, \vartheta_j, \varphi_k)$  grid of  $N_\xi \times N_\vartheta \times N_\varphi$  points ( $N_\xi = 64$ ,  $N_\vartheta = 32$ , and  $N_\varphi = 64$ , in typical applications), the  $\vartheta$  and  $\varphi$  derivatives are evaluated using the spectral representation of finite order Legendre-Fourier polynomials, and the radial derivatives are approximated by second order centered differences in the  $\xi_i$  coordinate. Thus, for each  $(l, m)$  the discretized operator  $\delta\hat{\mathcal{M}}_{l,m}^{(n)}$  to be inverted is represented by a pentadiagonal matrix over  $\xi_i$ . We note that for  $l > 0$  we solve equation (33) for  $\delta\phi_{l,m}^{(n)}$  with the boundary condition  $\delta\phi_{l,m}^{(n)}(\xi = \pi/2) = 0$ , while for  $l = 0$  equation (33) can be solved directly for the radial component of the acceleration increment.

#### 4.1. The tests

We tested the numerical code using the analytical axisymmetric and triaxial MOND models described in Section 3. We assigned the analytical density distribution obtained for

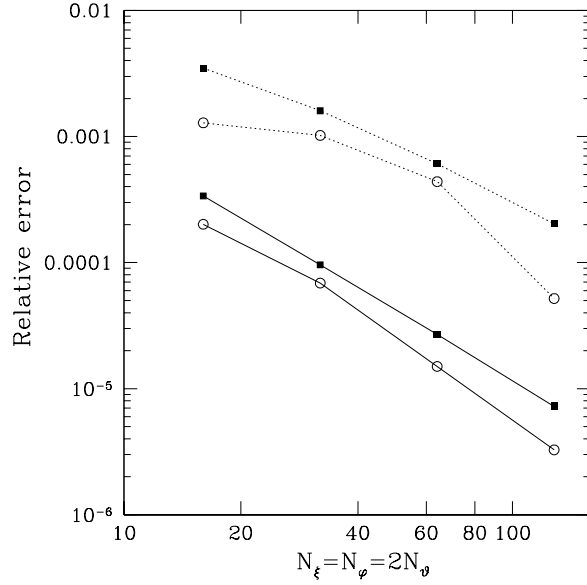


Fig. 5.— R.m.s. (solid line) and maximum (dotted line) relative error on the acceleration (calculated over all the space) as a function of the number of radial grid points  $N_\xi = N_\phi = 2N_\theta$  for two triaxial Hernquist models. Empty circles refer to the model with  $\phi_1$  in equation (21) with  $\beta = 5$ ,  $\tilde{\eta} = 0.02$  and  $\tilde{\epsilon} = 0.01$ , while solid squares to the model with  $\phi_1$  in equation (24) with  $\beta = 1$ ,  $\eta = 0.4$  and  $\epsilon = 0.2$ .

different values of  $a_0 r_c^2 / (GM_0)$ ,  $\epsilon$ ,  $\eta$ , and  $\beta$ , and we recovered the corresponding numerical MOND potential, comparing it with its analytical expression. The accuracy of the numerically estimated field  $\mathbf{g}_{\text{num}} \equiv -\nabla\phi_{\text{num}}$  is quantified by the relative error  $\|\mathbf{g} - \mathbf{g}_{\text{num}}\|/g$ , and in all the studied cases we found very good agreement between the analytical and numerical acceleration field, even for models near the consistency limit such as those in the bottom panels of Fig. 2 and 3. For example, in Fig. 5 we plot the r.m.s. (solid line) and maximum (dotted line) relative error calculated over all grid points, as a function of  $N_\xi = N_\phi = 2N_\theta$  for two triaxial Hernquist models: one with  $\phi_1$  as in equation (21) (empty symbols), the other with  $\phi_1$  as in equation (24) (solid symbols). It is apparent how the typical errors decrease down to values  $\sim 10^{-5}$ ; such values are reached in 15 – 20 iterations, taking few seconds on a common PC.

As a second set of tests, we studied the razor-thin Kuzmin disk (BM95). This is a quite severe test, because of the singular nature of the density distribution along the  $z$  direction. In this case, we found numerical convergence to the solution, with relative r.m.s. error

$5.6 \times 10^{-3}$  for  $N_\xi = N_\varphi = 128$ , and  $N_\theta = 64$ .

We note that our code converges also when dealing with multi-centered density distributions, for which the spherical grid is clearly not optimal. In such cases the convergence is not as fast as in the case of density distributions centered in the origin. For example, the MOND fields of groups of 2, 3, and 4 Hernquist spheres are computed in 20 – 25 iterations, with tolerance  $\varepsilon \sim 10^{-5}$ ,  $N_\xi = 64$ ,  $N_\theta = 32$ , and  $N_\varphi = 64$ .

As an illustrative application of the code, we evaluated the dMOND field for the family of homeoidally stratified triaxial Hernquist models

$$\rho = \frac{M_0}{2\pi r_c^3(1-\epsilon)(1-\eta)m(1+m)^3}, \quad (36)$$

where

$$m^2 = \frac{x^2}{r_c^2} + \frac{y^2}{r_c^2(1-\epsilon)^2} + \frac{z^2}{r_c^2(1-\eta)^2}, \quad (37)$$

and we investigated their solenoidal field for different flattenings. For example, the model in Fig. 4 (bottom panels) has  $\epsilon = 0$  and  $\eta = 0.5$ . The global behavior of  $\mathbf{S}$  is similar to what found for the analytical models of Section 3, with the larger contribution of  $\mathbf{S}$  near the center. In this case we found maximum values of  $S/g_N \sim 0.3$ . Even larger values were found for more flattened models: for instance,  $0.2 \lesssim S/g_N \lesssim 0.6$  in the central regions ( $r \lesssim r_c$ ) of a triaxial model with  $\eta = 0.8$ ,  $\epsilon = 0.6$ . This is curious because BM95 found similar values of  $S/g_N$  only in the quite artificial case of disks with a central hole. This last result suggests that when studying MOND equilibrium models for disks or elliptical galaxies it could be dangerous to solve equation (7) just relying on the *Ansatz* that in any case  $\mathbf{S}$  would be small.

## 5. Summary and conclusions

In this paper we presented a few representative axisymmetric and triaxial density models, both analytical and numerical, obeying the MOND field equation. The analytical density-potential pairs are constructed by means of a simple method based on the deformation of the potential of spherically symmetric systems. We show that in this way it is possible to build systems with radial profiles and shapes similar to those of real galaxies. Our method, although applied in the present paper by using simple deformations is easily generalizable to more complicated cases. As a complement to the analytical method, we also presented a numerical code (based on spectral methods) to solve the MOND field equation. We tested

the code against the new analytical triaxial models and the MOND Kuzmin disk, with excellent results in terms of both computational time and accuracy of the numerical solution. As a first simple application of the code, we explored the relevance of the solenoidal field  $\mathbf{S}$  in MOND distributions. Though we confirm that this field is typically small compared to the Newtonian field of the density distribution, we also found that for some systems  $\mathbf{S}$  is certainly not negligible, at least in some regions of space.

A particularly important application of the numerical solver will be its implementation in a particle-mesh N-body code. Such an implementation is promising, because our MOND solver is based on an iterative scheme, and at each time in a N-body simulation the potential at the previous time is a very good seed for the iterative procedure that should converge efficiently. More immediate possible applications of the presented analytical models and numerical code are the study of MOND orbits in aspherical density distributions, and the vertical motions of stars near the galactic plane. We conclude by pointing out that the developed numerical code can also be used to solve the equation for the scalar field in the non-relativistic limit of TeVeS, the relativistic MOND theory introduced by Bekenstein (2004; equation 53), allowing, for example, to investigate MOND gravitational lensing from non-spherical lenses.

We are grateful to James Binney, Hongsheng Zhao, and the anonymous referee for very useful comments. This work was partially supported by a MIUR grant CoFin2004.

### A. Three existence theorems

We present here three existence theorems that are at the basis of the technique presented in Section 2. The first result holds in general, while the second and third results assume spherical symmetry.

**Theorem 1** *Let  $\phi_N$  the Newtonian potential generated by a positive density distribution, i. e.*

$$\nabla^2 \phi_N \geq 0 \tag{A1}$$

*over the whole space. If*

$$\nabla \cdot (|\nabla \phi_N| \nabla \phi_N) \geq 0 \tag{A2}$$

over the whole space, then also

$$\nabla \cdot \left[ \mu \left( \frac{\|\nabla \phi_N\|}{a_0} \right) \nabla \phi_N \right] \geq 0, \quad (\text{A3})$$

where  $\mu$  is given in equation (5).

**Proof** Equation (A3) can be rewritten as

$$\nabla \cdot \left[ \mu \left( \frac{g_N}{a_0} \right) \nabla \phi_N \right] = \frac{1}{\sqrt{a_0^2 + g_N^2}} \left( g_N \nabla^2 \phi_N + \frac{\nabla g_N \cdot \nabla \phi_N}{1 + g_N^2/a_0^2} \right), \quad (\text{A4})$$

from condition (A1) a negative density can be produced only in the region of space  $\Omega^-$  where  $\nabla g_N \cdot \nabla \phi_N < 0$ . If  $\Omega^- = \emptyset$  the theorem is proved, thus let  $\Omega^- \neq \emptyset$ . In this case, by expansion of inequality (A2) we have that on  $\Omega^-$

$$g_N \nabla^2 \phi_N \geq -\nabla g_N \cdot \nabla \phi_N \geq -\frac{\nabla g_N \cdot \nabla \phi_N}{1 + g_N^2/a_0^2}, \quad (\text{A5})$$

and this proves the theorem.

We now prove a consequence of Theorem 1 holding for spherically symmetric systems, which is relevant to the construction of exact aspherical MOND solutions.

**Theorem 2** *Let  $\phi(r)$  the dMOND potential of a spherically symmetric (positive) density distribution. Then*

$$\nabla^2 \phi \geq 0, \quad (\text{A6})$$

and

$$\nabla \cdot \left[ \mu \left( \frac{\|\nabla \phi\|}{a_0} \right) \nabla \phi \right] \geq 0, \quad (\text{A7})$$

over the whole space.

**Proof** Direct calculation of  $\nabla^2 \phi$  in spherical symmetry, as done in equation (9), proves equation (A6). Conditions (A1) and (A2) are then verified and this proves equation (A7).

Note that the converse of Theorem 2 is not true, i.e.,  $\nabla^2 \phi \geq 0$  is not a sufficient condition for  $\nabla \cdot (\|\nabla \phi\| \nabla \phi) \geq 0$ . In fact, the following result holds

**Theorem 3** *Let*

$$\nabla^2 \phi = 4\pi G \rho(r) \geq 0. \quad (\text{A8})$$

*Then*

$$\nabla \cdot (\|\nabla \phi\| \nabla \phi) \geq 0, \quad (\text{A9})$$

*if and only if*

$$\rho(r) \geq \frac{M(r)}{4\pi r^3} \quad \forall r. \quad (\text{A10})$$

**Proof** The proof is obtained by expanding inequality (A9) in spherical symmetry as

$$\frac{d\phi}{dr} \left( \frac{d^2\phi}{dr^2} + 4\pi G\rho \right) \geq 0 : \quad (\text{A11})$$

the identity  $d\phi/dr = GM(r)/r^2$  proves the theorem.

## REFERENCES

- Bekenstein, J. 2004, Phys. Rev. D, 70, 083509
- Bekenstein, J., & Milgrom, M. 1984, ApJ, 286, 7
- Binney, J. 1981, MNRAS, 196, 455
- Binney, J., & Tremaine, S. 1987, Galactic Dynamics, Princeton University Press, Princeton
- Brada, R., & Milgrom, M. 1995, MNRAS, 276, 453 (BM95)
- Brada, R., & Milgrom, M. 1999, ApJ, 519, 590
- Buote, D.A., Jeltema, T.E., Canizares, C.R., & Garmire, G.P. 2002, ApJ, 577, 183
- Ciotti, L., & Bertin, G. 2005, A&A, 437, 419 (CB05)
- Ciotti, L., & Binney, J. 2004, MNRAS, 351, 285
- Dehnen, W. 1993, MNRAS, 265, 250
- de Vaucouleurs, G. 1948, Ann. d’Astroph., 11, 247
- Evans, N.W. 1994, MNRAS, 267, 333
- Famaey, B., & Binney, J. 2005, MNRAS, in press (astro-ph/0506723)
- Felten, J.E. 1984, ApJ, 286, 3
- Hernquist, L. 1990, ApJ, 356, 359

- Jaffe, W. 1983, MNRAS, 202, 995
- King, I.R. 1972, ApJ, 174, L123
- Knebe, A., & Gibson, B.K. 2004, MNRAS, 347, 1055
- Londrillo, P., & Messina, A. 1990, MNRAS, 242, 595
- Milgrom, M. 1983, ApJ, 270, 365
- Milgrom, M. 1986, ApJ, 302, 617
- Milgrom, M. 2002, New. Astron. Rev., 46, 741
- Miyamoto, M., & Nagai, R. 1975, PASJ, 27, 533
- Muccione, V., & Ciotti, L. 2004, A&A, 421, 583
- Plummer, H.C. 1911, MNRAS, 71, 460
- Sanders, R.H. 2003, MNRAS, 342, 901
- Sanders, R.H., & McGaugh, S.S. 2002, ARA&A, 40, 263
- Satho, C. 1980, PASJ, 32, 41
- Stoer, J., & Bulirsch, R. 1980, Introduction to Numerical Analysis (New York: Springer-Verlag)
- The, L.S., & White, S.D.M. 1988, AJ, 95, 1642
- Tremaine, S., Richstone, D.O., Yong-Ik, B., Dressler, A., Faber, S.M., Grillmair, C., Kormendy, J., Laurer, T.R. 1994, AJ, 107, 634
- Zhao, H., Bacon, D. J., Taylor, A.N., Horne, K. 2005, preprint (astro-ph/0509590)